Journal of Materials Chemistry C

Accepted Manuscript

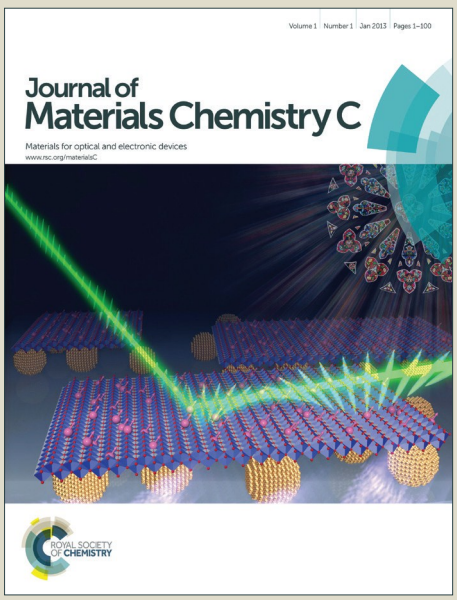

ROYAL SOCIETY OF CHEMISTRY

www.rsc.org/materialsC

Modulation of Thulium Upconversion in Potassium Tetraphosphates ($KLaP_4O_{12}$) nanocrystals by co-doping with Yb^{3+} ions

L. Marciniak[1*], A. Bednarkiewicz[1], M. Stefanski[1], R. Tomala[1], D. Hreniak[1], W. Strek[1]

[1]Institute of Low Temperature and Structure Research, Polish Academy of Sciences, Okólna 2, 50-422 Wroclaw, Poland

* corresponding author: l.marciniak@int.pan.wroc.pl

KEYWORDS tetraphosphates, up-conversion, NIR-to-NIR conversion

Abstract

The influence of sensitizer concentration on up-converting properties of $KLa_{0.99-x}Tm_{0.01}Yb_xP_4O_{12}$ nanocrystals were investigated in a wide range of Yb^{3+} concentration (x=0.05 – x=0.5). This impact was manifested by Yb^{3+} concentration dependent variation of up-conversion emission spectra, blue to NIR emission ratio variation, luminescence decay times as well as on orders of upconversion process. The observed processes of energy transfer between Yb^{3+} and Tm^{3+} was discussed in terms of reduction of average distance between dopants, $Tm^{3+} \rightarrow Yb^{3+}$ back energy transfer and energy migration to surface quenchers over Yb^{3+} sublattice.

Introduction

Growing interest of the possibility to employ luminescent nanoparticles (NP) for bioapplication can be attributed to their multifunctionality which enables combining a few tools, such as labeling capability for bioimaging[1-6], noncontact temperature measurements at subcellular or tissue level[7-8], light induced hyperthermia, photodynamic therapy etc. together into single particle. Due to their small size and feasibility of their biofunctionalization, NPs can be easy incorporated into biological probe for both *in vivo* as well as *in vitro* measurements[9-11]. Owing to the optical window biological tissues (750-1000 nm), NIR absorbing and NIR emitting luminescent labels are sought, which makesYb^{3+},Tm^{3+} codoped systems to be of great interest for many biomedical applications.

Most of the studies concerning UCNPs for bioimaging are based on fluorides (e.g. LaF_3, $NaYF_4$), because these materials possess high emission efficiency associated with low phonon energy[12-17]. Although considered as non-toxic, fluorides may display some chemical toxicity[18]. Therefore the phosphates which are the building material of bones and which

reveals much higher biocompatibility can be considered as a luminescent materials of choice for bioimaging. Moreover, one of the most important disadvantages of UC NPs is their low emission efficiency. UC emission intensity cannot be improved by increasing the activator ions concentration due to cross-relaxation processes which take place between dopants and lead to quenching of the luminescence. Therefore other approach to enhance the up-conversion intensity is based on increasing of the absportion cross section for excitation wavelength by increasing the concentration of sensitizer ions (here Yb^{3+})[19]. As it was already proven by us that tetraphosphate hosts[20], due to significantly larger distance between dopants (6A comparing to 3 A or less for fluorides), allows for higher doping level without undesirable luminescence concentration quenching even for stoichiometric compounds.

The biological utility of the studied material comes from the possibility to increase the dopant concentrations without severe concentration quenching. This feature originates from long distances between Ln^{3+} impurities and increases both absorption or emission/up-conversion cross section, which is of utmost importance for biomedical applications. Of course, the ultimate goal, i.e. the possibility to apply this material in bio-assays and bio-imaging is strongly related to many factors such as up-conversion efficiency (which is a complex relation between available phonons, NPs size and anisotropy of shape, dopant concentration and interplay between sensitizers and activators etc.), bio-compatibility, available bio-functionalization protocols etc.. Current work is focused on chemical and spectroscopic studies on this promising material. Recently we have published the results of up-conversion properties of $KLa_{0.95-x}Er_{0.05}Yb_xP_4O_{12}$ and $La_{0.95-x}Er_{0.05}Yb_xP_5O_{14}$ nanocrystals[19], which revealed the concentration of Yb^{3+} ions plays a significant role and impacts the red to green emission intensities ratio as well as the luminescence decay times of UC emission. These two premises motivated us to systematically study the impact of Yb^{3+} ions concentration on the Vis-to-NIR emission bands of Tm^{3+} activators in $KLa_{0.99-x}Tm_{0.01}Yb_xP_4O_{12}$ nanocrystals.

Experimental

$KLa_{0.99-x}Tm_{0.01}Yb_xP_4O_{12}$ nanocrystals were successfully synthesized using previously described co-precipitation method[18, 20]. K_2CO_3 (potassium carbonate, Aventor, pure), La_2O_3, Yb_2O_3, Tm_2O_3 (of 99.999 %, 99.998 % 99.999 % purity respectively from Stanford Materials Corporation), $(NH_4)_2HPO_4$ (ammonium phosphate dibasic, Sigma Aldrich, ≥99.99 %) were used as starting materials. Potassium carbonate and all of lanthanide oxides (Ln_2O_3) were dissolved in deionized water with addition of HNO_3 in separate glasses. After triple recrystallization, nitrates of potassium and lanthanides were mixed together and added to the

water solution of ammonium phosphate dibasic. In result white suspension was obtained and dried for 3 days at 90 ^{o}C. Finally, obtained powders were annealed for 6 h at 450^{o}C. In order to analyze the influence of the Yb^{3+} concentration on the spectroscopic properties of tetraphosphates the concentration of Tm^{3+} was set as 0.05 and the Yb^{3+} concentration was changed in range from x=0.05 to x=0.5 in respect of La^{3+} ions.

Powder diffraction studies were carried out on PANalytical X'Pert Pro diffractometer equipped with Anton Paar TCU 1000 N Temperature Control Unit using Ni-filtered Cu *Kα* radiation (V = 40 kV, I = 30 mA).

Transmission electron microscope images were taken using FEI Tecnai G^2 20 X-TWIN microscope supplied with CCD FEI Eagle 2K camera with HAADF detector and electron gun with LaB_6 cathode. Moreover microscope was supplied with X-ray microanalyzer EDAX.

The emission spectra were measured using FLS980 Fluorescence Spectrometer from Edinburgh Instruments. Both the excitation and emission 300 mm focal length monochromators were in Czerny Turner configuration. Emission arm was supplied with ruled grating, 1800 lines/mm blazed at 500 nm. The spectral resolution was 0.1 nm. Two types of detector were used: R928P side window photomultiplier tube from Hamamatsu. The 980 nm line from laser diode (LD) was used as an excitation.

The luminescence kinetics measurements were performed using Jobin-Yvon HR1000 monochromator equipped with R928P photomultiplier tube from Hamamatsu and using 980 nm line pulsed work (PW) from Ti:Sapphire laser as an excitation source. The decay profiles were collected using a LeCroy WaveSurfer 400 oscilloscope.

Results and discussion

The potassium lanthanum tetraphosphates ($KLaP_4O_{12}$) crystallizes in the monoclinic structure of P 1 21 1 (4) symmetry and following cell parameters: a=8.106 Å, b=8.551 Å, c=7.326 Å, □=92.18^{o}, V=507.43 Å^3 and Z=2. Due to the fact that the LaO_8 dodecahedrons are separated to each other by helical chains of $(PO_4)^{3-}$ tetrahedral the average distance between lanthanum ions is La^{3+}-La^{3+}=6.65 Å. Since the dopant ions of lanthanides substitutes the La^{3+} sites in the structures due to the comparable ionic size and the charge, the dopants are relatively well separated to each other. Hence the energy transfer processes which can appears between dopants are reduced. There is only one crystallographic site of La^{3+} (symmetry C_1) in the $KLaP_4O_{12}$ host. In order to determine the influence of the sensitizer concentration on the

up-conversion properties of $KLa_{0.99-x}Tm_{0.01}Yb_xP_4O_{12}$ nanocrystals the series of powders with different Yb^{3+} concentration was prepared (x=0.05, x=0.1, x=0.2, x=0.3 and x=0.5). The powder X-ray diffraction data of the obtained powders were presented in Fig. 1a. The spectra consists of series of diffraction peaks attributed to monoclinic $KLaP_4O_{12}$ structure (ICSD 33241). The characteristic broadening of the XRD peaks results of small size of the nanocrystals. Any influence of the Yb^{3+} concentration on the cell parameters of the $KLa_{0.99-x}Tm_{0.01}Yb_xP_4O_{12}$ was found. The images from transmission electron microscopy (TEM) of the $KLa_{0.99-x}Tm_{0.01}Yb_xP_4O_{12}$ nanocrystals is presented in Fig. 1b,c. One can see well crystallized, aggregated grains of the size around 25 nm. The grain size distribution is presented in Fig. 1c.

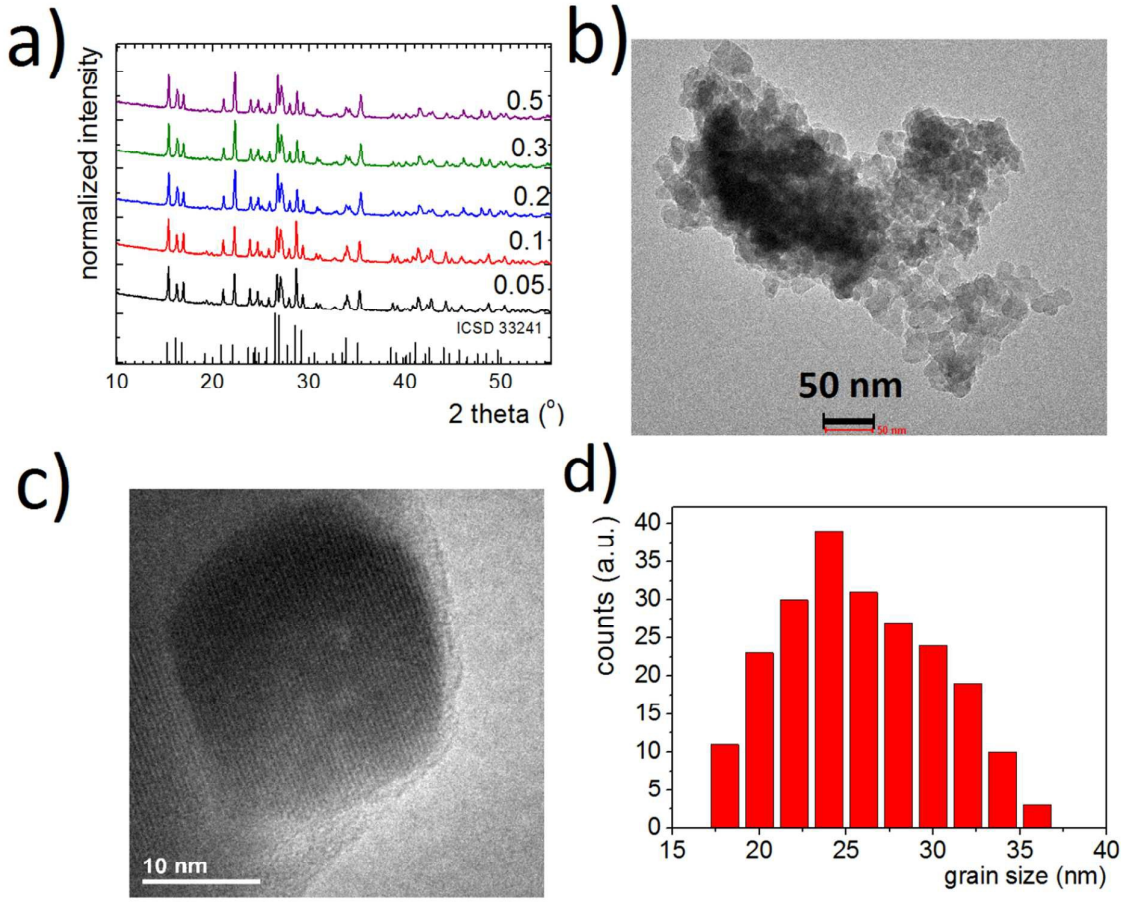

Figure 1. Characterization of structure and morphology of $KLa_{0.99-x}Tm_{0.01}Yb_xP_4O_{12}$ nanocrystals: the X-ray diffraction patterns – a; the transmission electron microscopy image –b, c; and the grain size distribution –d.

The up-conversion (UC) emission spectra of $KLa_{0.99-x}Tm_{0.01}Yb_xP_4O_{12}$ nanocrystals were measured in range 400-900 nm under λ_{exc}=980 nm. Excitation line corresponds to the absorption of Yb^{3+} ions ($^2F_{7/2} \rightarrow {}^2F_{5/2}$ transition). The UC spectra measured for different Yb^{3+}

concentration are presented in Fig. 2a. The dominant band localized at 798 nm is associated with $^3H_4 \rightarrow {}^3H_6$ transition of Tm^{3+} ion. Another three emission bands found at 475, 647 and 683 nm can be associated with $^1G_4 \rightarrow {}^3H_6$, $^1G_4 \rightarrow {}^3F_4$ and $^3F_2 \rightarrow {}^3H_6$ electronic transitions. The increase of the Yb^{3+} concentration results in enhancement of the up-conversion emission intensity. One can see in Fig. 1b that blue to NIR emission intensities ratio increases sublinearly with rising Yb^{3+} concentration and the ratio for x=0.5 is over 3 times larger as compared to the initial x=0.05 concentration of the sensitizer. The augmentation of Yb^{3+} concentration causes faster increase of bands in Vis part of spectra comparing to the NIR one. Emission intensities of each of emission band in respect to total emission intensity as a function of Yb^{3+} concentration is presented in Fig. 2c. Intensity of $^3H_4 \rightarrow {}^3H_6$ decreases around 20% witch Yb^{3+} concentration. This behavior may suggest $Tm^{3+} \rightarrow Yb^{3+}$ back energy transfer (BET), which will be discussed later on. From the other hand all of emission bands reveals enhancement with enlarging sensitizer concentration. The most remarkable enlargement was found for $^3F_2 \rightarrow {}^3H_6$ transition (c.a.800%), however for other bands increase is also considerable (for $^1G_4 \rightarrow {}^3H_6$ (c.a.200 %) , $^1G_4 \rightarrow {}^3F_4$ (c.a.175%). Therefore the NIR to blue up-conversion emission intensity ratio can be easily controlled by the Yb^{3+} concentration.

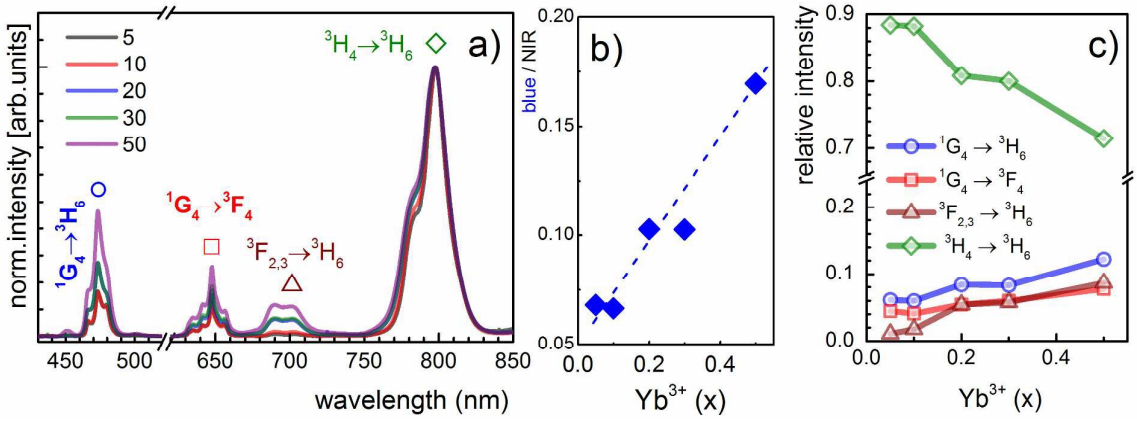

Figure 2. Up-conversion emission spectra of $KLa_{0.99-x}Tm_{0.01}Yb_xP_4O_{12}$ – a; blue to NIR emission intensities ratio –b; and relative emission intensities of particular emission bands in a function of Yb^{3+} concentration –c.

To explain these trends, the hypothetical energy transfer processes which take place in Yb^{3+}, Tm^{3+} codoped nanocrystals are presented in Fig. 3. The excitation 975 nm line is absorbed by Yb^{3+} ions leading to the population of excited state $^2F_{5/2}$ of Yb^{3+} ions (process 1, Fig. 3) followed by the $Yb^{3+} \rightarrow Tm^{3+}$ energy transfer populating $^3H_5$ state (proc. 2, Fig. 3). After

nonradiative transition to $^3F_4$ term another $Yb^{3+} \rightarrow Tm^{3+}$ energy transfer may take place leading to $^3F_2$ population (proc. 3, Fig. 3) followed by nonradiative transition to $^3H_4$ state. From this state either radiative transition may take place (798 nm) or after another $Yb^{3+} \rightarrow Tm^{3+}$ energy transfer (proc. 4, Fig. 3) $^1G_4$ term can be populated from which via radiative relaxation 475 nm photon can be emitted. In this way all emitting state $^1G_4$, $^3F_{2,3}$ and $^3H_4$ are populated. However as it can be noticed, the order of multiphoton processes is considerable different for these states. $^3H_4$ can be populated via 2 photons of 980 nm or, in case of phonon assisted energy transfer with phonon absorption even by one photon, while respectively $^3F_{2,3}$ needs two and $^1G_4$ three incident NIR photons for being populated. Therefore, the probability of particular energy state population is significantly different according to general rule: the higher number of energy transfer which are involved in the population of emitting state, the lower is its probability. For low dopant concentration the average distance between Tm^{3+} and Yb^{3+} ions is relatively large. Hence in case of lowest 0.05 concentration of Yb^{3+} ions, the highest emission intensity can be observed for transition from $^3H_4$ state. The increase of sensitizer concentration leads to the gradual shortening of average distance between Tm^{3+} and Yb^{3+}, which enhances the probability of energy transfer between these ions and facilitates multiphoton energy transfers.

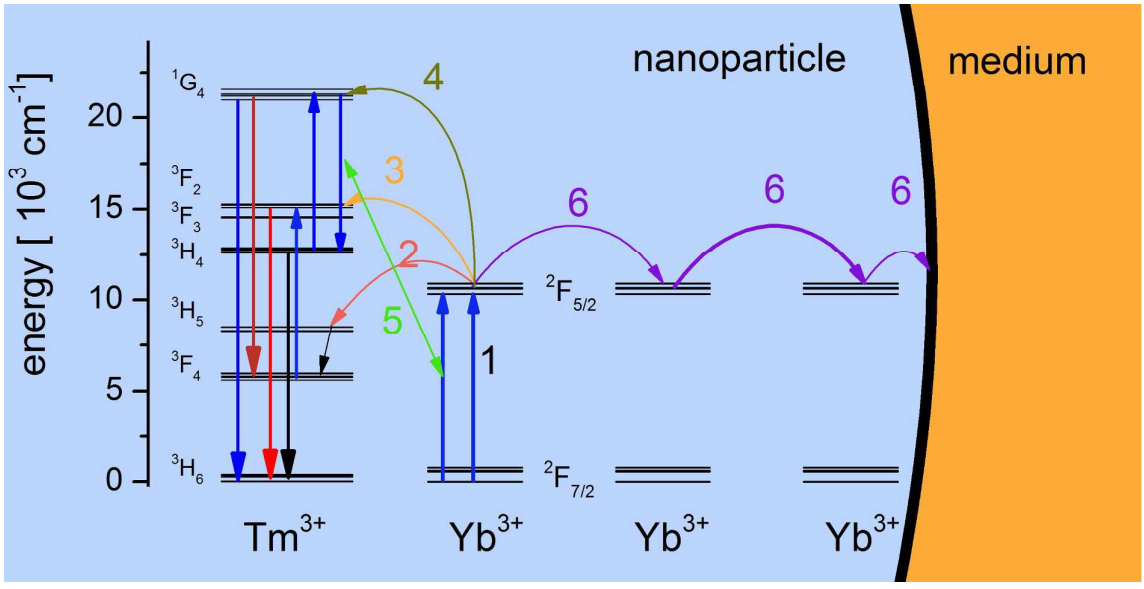

Figure 3. The energy diagram of energy transfers which take place in $KLa_{0.99-x}Tm_{0.01}Yb_xP_4O_{12}$ nanocrystals.

In order to understand the changes in the energy transfers which leads to tuning of NIR to blue emission intensity ratio in $KLa_{0.99-x}Tm_{0.01}Yb_xP_4O_{12}$ nanocrystals with sensitizer concentration the luminescence kinetics were investigated of blue and NIR emission of Tm^{3+}

and Yb^{3+} emission (Fig. 4). As it can be noticed, the luminescence decay profiles of Tm^{3+} both at 475 nm and 798 nm are characterized by rise time expected for energy transfer up-conversion process (ETU). The increase of Yb^{3+} concentration leads to shortening of decay times respectively from 300 μs to 180 μs for of blue emission and from 370 μs to 200 μs for NIR emission. Since the concentration of activators (emitting Tm^{3+} ions) is constant in each of the analyzed samples, the shortening of luminescence decay times should originate from the Tm^{3+} -Yb^{3+} interaction. Therefore, the observed shortening can be ascribed to back energy transfer from Tm^{3+} to Yb^{3+} (proc. 5 Fig. 3). Due to resonance between proper energy levels of Tm^{3+} with corresponding Yb^{3+} energy levels the increase of Yb^{3+} concentration results in enhancement of back energy transfers. It is also worth mentioning, that luminescence decay profiles of Yb^{3+} concentration decreases proportionally to the rising sensitizer concentration which shall be associated with two phenomena. The first one is related with shortening of Tm^{3+} to Yb^{3+} distance and hence the faster energy transfer from Yb^{3+} to Tm^{3+}. The second one results from increasing the probability of energy migration in the Yb^{3+} sublattice. In the latter case, the excitation energy can migrate among Yb^{3+} ions, and due to limited volume to surface ratio, rich the surface of the nanocrystal, where the excited states are subject to quenching on the surface defects and by the vibrations of molecules attached to the nanocrystal's surface like hydroxyl, carboxyl etc. (process #6 at Fig. 3).

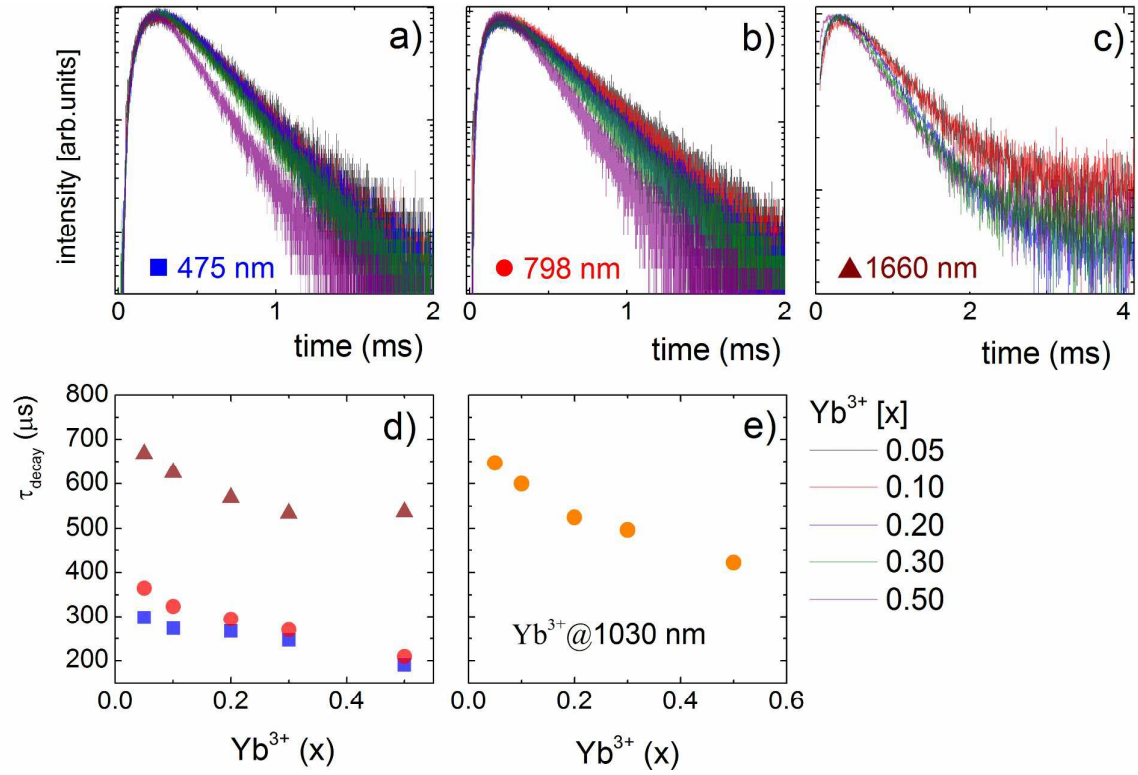

Figure 4. Luminescence decay profiles of $KLa_{0.99-x}Tm_{0.01}Yb_xP_4O_{12}$ nanocrystals measured for λ_{em}=475 nm- a, λ_{em}=798 nm – b; λ_{em}=1660 nm – c; and decay times of Tm^{3+} emission –d; and Yb^{3+} emission –e as a function of Yb^{3+} concentration.

In a course of up-conversion luminescence the emission intensity (I_{em}) strongly depends on the excitation power (P_{exc}) according to well known relation $I_{em} \sim P_{exc}^{N}$, where N expresses the number of the incident NIR photons involved in the generation of UC emission. However for due to the energy transfer that can take place between dopant ions the phenomenological UC orders obtained from emission power dependence studies represents the balance between UC population processes and the depopulation processes of excited states involving emission and nonradiatve depopulation. Hence the power dependence of emission intensity studies gives crucial information about the processes of origin of observed emission. Power dependence of intensity of emission at 475 nm, 683 nm and 798 nm associated with emission from $^1G_4$, $^3F_2$ and $^3H_4$ levels are presented in Fig. 5. The dependence of UC orders in a function of Yb^{3+} concentration is (determined for the power density in range 1-100 W/cm^2) presented in Fig. 5d. As it can be noticed, in case of low Yb^{3+} concentration the $^1G_4$ level is populated via three, while $^3F_2$ and $^3H_4$ via two photon processes, what is in agreement with common understanding of Yb-Tm upconversion and is presented in energy diagram in Fig. 3. However, the increase of Yb^{3+} concentration results in lowering of UC orders to two ($^1G_4$) and close to one in case of $^3F_2$ and $^3H_4$ energy levels. This is most probably the consequence

of the rising probability of back energy transfers which take place between Tm^{3+} and Yb^{3+} levels, which is obviously dependent on Yb^{3+} concentration. The phenomenological UC orders obtained from emission power dependence studies are representing the balance between UC population processes and few competing depopulation processes he of excited state such as emission, cross-relaxation and back energy transfer. Therefore, the observed lowering of UC order confirms previously postulated back energy transfer from Tm^{3+} to Yb^{3+}.

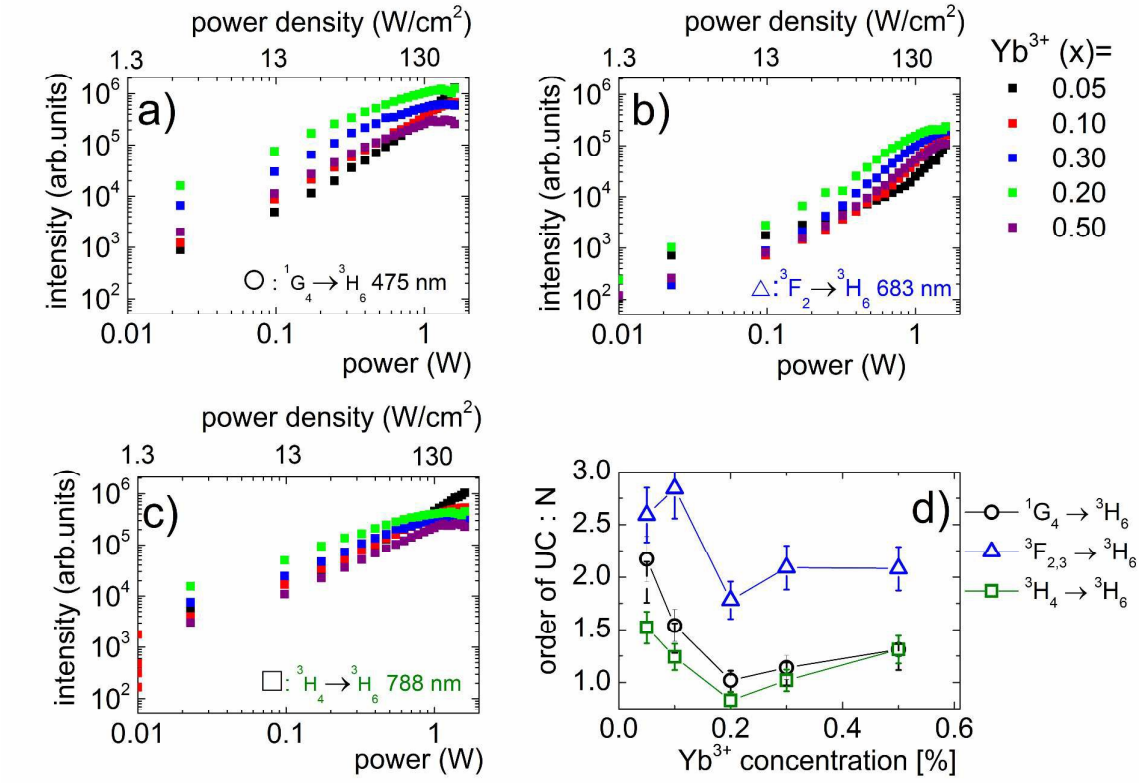

Figure 5. The power dependence of emission intensities in $KLa_{0.99-x}Tm_{0.01}Yb_xP_4O_{12}$ nanocrystals measured for λ_{em}=475 nm- a, λ_{em}=683 nm – b, λ_{em}=788 nm – c, and the dependence of UC orders as a function of Yb^{3+} concentration-d.

The influence of the sensitizer concentration on UC properties of Yb^{3+},Tm^{3+} codoped systems was previously described for other up-converting materials. Qiu et al was investigating spectroscopic properties YF_3:Tm,Yb nanodisks in a wide range of Yb^{3+} concentration (10-98%)[22]. It was found that high concentration of sensitizer favors five and four photon processes comparing to low-photon UC. Moreover increase of Yb^{3+} concentration results in continuous increase of blue emission intensity (for up to 90% of Yb^{3+}). Ostermayer et al. presented quantitative investigations of the influence of sensitizer concentration on UC of YF_4 single crystals[23]. The presented calculations confirms the results observed by us for $KLa_{0.99-x}Tm_{0.01}Yb_xP_4O_{12}$, i.e. the shortening of the Tm^{3+} to Yb^{3+} distance by increasing of Yb^{3+}

concentration increases the probability of emission from higher laying states. However after reaching some critical D-D and D-A distance, the back energy transfer will decrease the Tm emission with further Yb^{3+} concentration. Yin et al reported increase of blue to NIR emission intensity by more than one order of magnitude with increasing the Yb^{3+} concentration from 20% to 40% for hexagonal $NaYF_4$:Yb,Tm nanocrystals[24]. Zhai et al.[25] reported increase of the emission intensity of $NaTm_{0.02}Lu_{0.98-x}Yb_xF_4$ nanocrystals. Moreover authors presents shortening of decay times as well as small lowering of UC orders with increase of Yb^{3+} concentration. However observed changes were not as significant as in case of $KLa_{0.99-x}Tm_{0.01}Yb_xP_4O_{12}$ nanocrystals.

Conclusions

Synthesis and spectroscopic properties of $KLa_{0.99-x}Tm_{0.01}Yb_xP_4O_{12}$ nanocrystals in a wide range of sensitizer concentration (from x=0.05 to 0.5) were investigated. The blue to NIR emission intensities ratio was increased by the Yb^{3+} concentration due to increase of the population probability of higher laying energy states of Tm^{3+} with shortening of the average distance between Tm^{3+} and Yb^{3+} ions. The decay times of blue and NIR emission of Tm^{3+} undergo of shortening with Yb^{3+} concentration due to higher probability of back energy transfer from Tm^{3+} to Yb^{3+} for higher sensitizer concentration. Moreover the Yb^{3+} decay times slightly decrease with Yb^{3+} concentration due to energy migration through Yb^{3+} sublattice leading to Yb^{3+} intensity quenching on the surface defects. It was shown that the order of the UC processes was reduced for higher sensitizer amount due to the competition between population and depopulation of emitting state by inter ionic interaction between Tm^{3+} and Yb^{3+} ions. Higher amount of sensitizer ions reduces average distance between interacting ions what facilitates energy transfers between them. Presented results confirms that by simple change of sensitizer concentration the blue to NIR emission intensities ration can be tuned depending on the application type. Since NIR to NIR UC process is especially important for bioimaging and blue emission can be used as a trigger for PDT presented regulation of NIT to blue emission intensity ratio is attractive for bioapplication

Acknowledgements

L. M. acknowledges support from the NCN under grant no. 2012/05/N/ST5/02327. LM acknowledges financial support from the Foundation for Polish Science under START 2015 program.

References

[1] V. Mahalingam, F.Vetrone, R. Naccache, A. Speghini, J. A. Capobianco, Adv. Mater, 2009, 21, 4025-4028.
[2] Y. S. Liu, D. T. Tu, H. M. Zhu, E. Ma, X. Y. Chen, Nanoscale, 2013, 5, 1369-1384.
[3] S. Santra, J. S. Xu, K. M. Wang, W. H. Tan, J Nanoscience Nanotech, 2004, 4, 590-599.
[4] B. A. Holm, E. J. Bergey, T. De, D. J. Rodman, R. Kapoor, L. Levy, C. S. Friend, P. N. Prasad, Molec. Crystals Liquid Crystals, 2002, 374, 589-598.
[5] J. L. Yuan, G. L. Wang, Trac-Trends In Analytical Chemistry, 2006, 25, 490-500.
[6] P. Sharma, S. Brown, G. Walter, S. Santra, B. Moudgil, Advances In Colloid And Interface Science, 2006, 123-126, 471-485.
[7] D. Jaque, F. Vetrone Nanoscale 2012, 4, 4301-4326.
[8] D. Jaque, L. M. Maestro, E. Escudero, E. M. Rodriguez, J. A. Capobianco, F. Vetrone, A. J. de la Fuente, F. Sanz-Rodriguez, M. C. Iglesias-de la Cruz, C. Jacinto, U. Rocha, J. G. Sole, J Lumin, 2013, 133, 249-253.
[9] M. Saxena, S. Sarkar, Mater Express 2013, 3, 201-209.
[10] Y. Q. Wu, M. Shi, L. Z. Zhao, W. Feng, F. Y. Li, C. H. Huang, Biomaterials, 2014, 35, 5830-5839.
[11] S. K. Singh, RSC Advances, 2014, 4, 58674-58698.
[12] H. Lu, G. Yi, S. Zhao, D. Chen, L.-H. Guo, J.Cheng, J. Mater. Chem., 2004,14, 1336-1341
[13] N.-N. Dong, M. Pedroni, F. Piccinelli, G. Conti, A. Sbarbati, J.E. Ramirez-Hernandez, L.M. Maestro, M.C. Iglesias-de la Cruz, F. Sanz-Rodriguez, A. Juarranz, F. Chen, F. Vetrone, J.A. Capobianco, J.G. Sole, M. Bettinelli, D. Jaque, A. Speghini, ASC Nano, 2011, 5, 8665–8671
[14] M. Lin, Y. Zhao, S. Wang, M. Liu, Z. Duan, Y. Chen, F. Li, F. Xu, T. Lu, Biotechnol Adv., 2012, 30, 1551-1561.
[15] M. Deng, Y. Ma, S. Huang , G. Hu, L. Wang, Nano Res., 2011, 4, 685-694.
[16] G.S. Yi, W.B. Lee, G.M. Chow, J. Nanosci. Nanotechnol. 2007, 7, 2790-2794.
[17] X. Liu, X. Kong, Y. Zhang, L. Tu, Y. Wang, Q. Zeng, C. Li, Z. Shi, H. Zhang, Chem. Commun. 2011, 47, 11957-11959.
[18] A. Gnach, A. Bednarkiewicz, Nano Today, 2012, 7, 532–563.
[19] A Brenier, G Boulon, J Alloy Compd, 2001. 323–324, 210-213.
[20] L. Marciniak, M. Stefanski, R. Tomala, D. Hreniak, W.Strek, J Chem Phys 2015, 143, 094701-1 – 094701-10.
[21] L Marciniak, W Strek, Y Guyot, D Hreniak, Phys Chem Chem Phys 2014, 16, 18004-18009.
[22] H. L. Qiu, G. Y. Chen, R. W. Fan, L. M. Yang, C. Liu,S. W. Hao, M. J. Sailor, H. Agren, C. H. Yang and P. N.Prasad, Nanoscale, 2014, 6, 753–757.
[23] F. W. Ostermayer, Jr., J. P. van der Ziel, H. M. Marcos, L. G. Van Uitert, and J. E. Geusic Phys. Rev. B 3, 1971, 2698-2705.
[24] A. X. Yin, Y. W. Zhang, L. D. Sun and C. H. Yan, Nanoscale,2010, 2, 953–959.
[25] X. S. Zhai, S. S. Li, Y. L. Zhang, G. S. Qin and W. P. Qin, J. Mater. Chem. C, 2014, 2, 2037–2044.